INSTITUTE OF PHYSICS PUBLISHING MODELLING AND SIMULATION IN MATERIALS SCIENCE AND ENGINEERING

Modelling Simul. Mater. Sci. Eng. **12** (2004) 1017–1029 PII: S0965-0393(04)80080-9

Analysis of shear deformations in Al and Cu: empirical potentials versus density functional theory

Robert D Boyer[1], **Ju Li**[3], **Shigenobu Ogata**[2,4,5] **and Sidney Yip**[1,2,6]

[1] Department of Materials Science and Engineering, Massachusetts Institute of Technology, Cambridge, MA 02139, USA
[2] Department of Nuclear Engineering, Massachusetts Institute of Technology, Cambridge, MA 02139, USA
[3] Department of Materials Science and Engineering, Ohio State University, Columbus, OH 43210, USA
[4] Department of Mechanical Engineering and Systems, Osaka University, Osaka 565-0871, Japan
[5] Handai Frontier Research Center, Osaka University, Osaka 565-0871, Japan

E-mail: syip@mit.edu

Received 21 April 2004
Published 9 August 2004
Online at stacks.iop.org/MSMSE/12/1017
doi:10.1088/0965-0393/12/5/017

Abstract

Multiplane shear deformation behaviour in face-centred cubic metals, aluminium and copper, is studied and empirical many-body potential results are directly compared with *ab initio* electronic structure calculations. An analysis of stress–displacement, atomic relaxation, and gamma-surface for $\{111\}\langle 11\bar{2}\rangle$ shear indicates that the potential for copper proposed by Mishin is able to capture the essential deformation behaviour. For aluminium the Mishin potential gives better results than the Ercolessi model in atomic relaxation and stress–displacement, although there remain details that neither are able to describe. Aluminium presents a greater challenge to empirical potential description because of the directional nature of its interatomic bonding.

(Some figures in this article are in colour only in the electronic version)

1. Background/motivation

Ideal shear stress–strain behaviour is fundamental to understanding the mechanical behaviour of a material. The maximum shear stress achievable in a crystal is the ideal shear strength, which often marks the shear-driven breaking of nearest-neighbour (NN) bonds. This is a microscopic process that occurs every time a dislocation core moves, reconfigures, or is nucleated, although in an asynchronous and inhomogeneous manner. Density functional theory (DFT) (Hohenberg and Kohn 1964, Kohn and Sham 1965) provides powerful tools for

[6] Author to whom any correspondence should be addressed.

the study of the ideal strength behaviour of materials because of its ability to accurately model the process of bonds breaking and reforming (Kioussis *et al* 2002). However, tracking valence electron densities requires significant computational effort. The study of plastic deformation mechanisms, such as dislocation nucleation and migration, requires larger length and time scales than are typically accessible to *ab initio* calculations. Empirical potentials allow for faster calculation by following only atomic degrees of freedom explicitly and, as a result, larger and more complicated systems can be treated, with certain reductions in accuracy. By fitting to a wide array of *ab initio* data as well as experimentally derived properties, potentials have been developed to capture increasingly more complex behaviour pertaining to interatomic bond breaking and its consequences. Benchmarking empirical potentials with *ab initio* calculations can determine how well an empirical potential can account for the essential behaviour of shear deformation.

2. Methods

2.1. Empirical potentials

The empirical potentials considered in this study are members of a class of potentials based on the 'Embedded Atom Method' (EAM) that derives its name from the description of metals as atoms 'embedded' in a cloud of electrons that generates bonding. Standard EAM potentials contain a pair-wise interaction term and an additional term to account for the local electron density surrounding each atom; they take the following form:

$$E = \sum_i G_i \left(\sum_{j \neq i} \rho_j(r_{ij}) \right) + \frac{1}{2} \sum_{i,\neq j} V(r_{ij}), \tag{1}$$

where G_i is the embedding function, ρ_j is the electron density calculated as a sum of contributions from neighbouring atoms, and $V(r_{ij})$ is the pair-wise interaction. A wide range of fitting schemes have been employed to develop physically meaningful potentials for a variety of metallic systems. In general, one or both of the terms in the potential are fitted to empirical data such as lattice constants, cohesive energy and elastic constants. More recently, the practice is to generate a database by first-principles DFT calculations and to fit a postulated potential form or spline functions to this database. We will study two potentials for aluminium, developed by Ercolessi and Adams (1994) and by Mishin *et al* (1999), and a subsequent potential for copper, developed by Mishin *et al* (2001).

2.2. Static calculation setup

For all empirical potential calculations the initial fcc supercell was built with the x, y and z-axes along $\langle 11\bar{2} \rangle$, $\langle \bar{1}10 \rangle$ and $\langle 111 \rangle$ directions, respectively. For relaxed and unrelaxed affine shear, periodic boundary conditions are imposed. In relaxed shear calculations, stress components other than the imposed σ_{13} are relaxed by conjugate gradient Press *et al* (1996) energy minimization with respect to the supercell shape and dimensions. The observed relaxation can be directly related to the atomic mechanism for accommodating shear (Ogata *et al* 2002) and it is of interest to determine the extent to which empirical potentials can capture this detailed behaviour.

The generalized stacking fault energy has long been used to describe material deformation in terms of the energy penalty for shearing two adjacent planes (Vitek 1968). Recently the multiplane generalized stacking fault energy has also been introduced to describe the energy penalty incurred when an arbitrary number of planes, n+1, are sheared relative to the adjacent

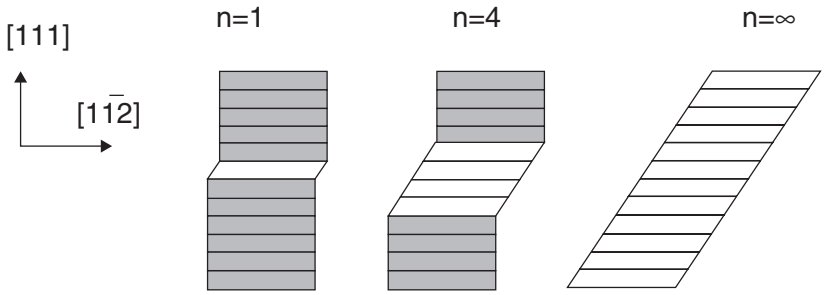

Figure 1. Schematic illustrating examples of the multiplane generalized stacking fault energy: $n = 1$, the generalized stacking fault energy, $n = 4$, multiple slipped planes and $n = \infty$, affine shear deformation.

plane by a common displacement, $\boldsymbol{x}$, that lies in the slip plane (see figure 1) (Ogata *et al* 2002). This quantity is given by

$$\gamma_n(\boldsymbol{x}) = \frac{E_n(\boldsymbol{x})}{nS_0}, \qquad n = 1, 2, \ldots, \tag{2}$$

where $E_n(\boldsymbol{x})$ is the strain energy at displacement $\boldsymbol{x}$ relative to its value at $\boldsymbol{x} = 0$, S_0 the cross-sectional area on which shearing is taking place and n the number of adjacent planes being sheared. The $n = 1$ case, $\gamma_1(\boldsymbol{x})$, corresponds to the conventional generalized stacking fault energy, while strain energy for affine shear is $\gamma_\infty(\boldsymbol{x})$.

The multiplane generalized stacking fault energy was the basic quantity that we calculated using empirical potentials and DFT. From this we derive corresponding stress–displacement response curves as defined by $\mathrm{d}\gamma_n(\boldsymbol{x})/\mathrm{d}\boldsymbol{x}$. The calculation of $\mathrm{d}\gamma_n(\boldsymbol{x})/\mathrm{d}\boldsymbol{x}$ was performed using a supercell containing thirty-six $\{111\}$ planes with free surfaces in the $\langle 111\rangle$ direction and periodic boundary conditions in the two in-plane directions. The undeformed crystal regions above and below the series of stacking faults are constrained to move as rigid blocks. Comparison of the stress–displacement responses, particularly for $n = 1$ and $n = \infty$, allows one to scrutinize the efficacy of the empirical potentials in accounting for the mechanistic details of the deformation behaviour. The information extracted in this manner can be further correlated with atomic relaxation patterns given by the empirical potentials and DFT. Another useful comparison which we will also examine is between aluminium and copper; this will give a measure of the relative degree of directional bonding between the two metals (Ogata *et al* 2002).

2.3. DFT calculation setup

We perform DFT calculations using the Vienna *ab initio* simulation package (Kresse and Hafner 1993). The exchange-correlation density functional adopted is the Perdew–Wang generalized gradient approximation (GGA) (Perdew *et al* 1992). An ultrasoft (US) pseudopotential (Vanderbilt 1990) is used. The cut-off energies for the plane wave basis set for Al and Cu are 162 eV and 292 eV, respectively. The Brillouin zone (BZ) k-point sampling is performed using the Monkhorst–Pack algorithm (Monkhorst and Pack 1976) whose convergence is carefully monitored. The BZ integration follows the Methfessel–Paxton scheme (Methfessel and Paxton 1989) with the smearing width being chosen so the entropic free energy ('-TS' term) is less than 0.5 meV per atom. In the relaxed affine shear calculations, subsidiary stress components are relaxed to within a convergence tolerance of 0.05 GPa.

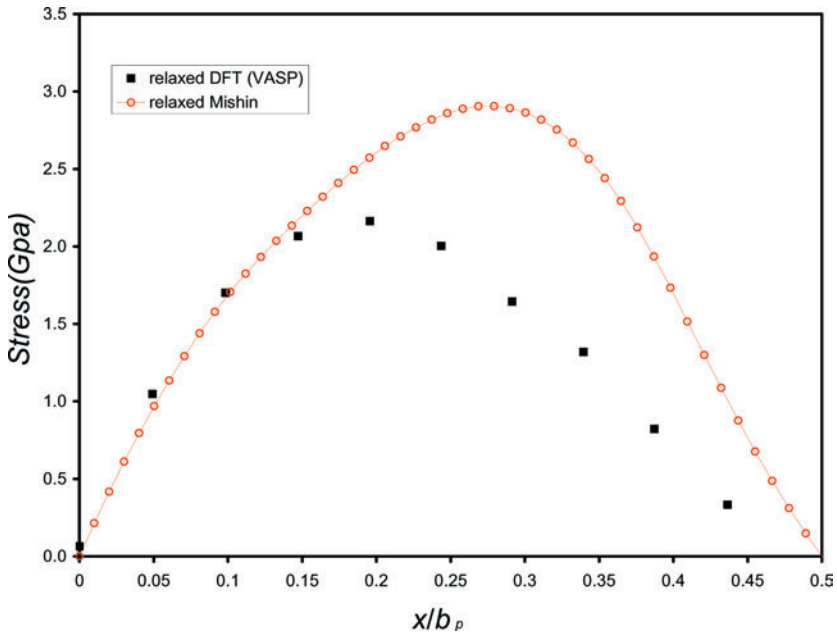

Figure 2. $\{111\}\langle 11\bar{2}\rangle$ pure shear stress–displacement response for copper using the Mishin copper potential (○) and DFT (■).

3. Results/discussion

The relaxed $\{111\}\langle 11\bar{2}\rangle$ stress–displacement response for copper calculated with the Mishin copper potential is shown in figure 2. The calculated displacements are normalized by the partial Burgers vector, $\boldsymbol{b}_\mathrm{p} = a_0[11\bar{2}]/6$, where a_0 is the equilibrium lattice parameter for the potential in use. The normalization allows the direct comparison of strain deformation between the empirical potential and DFT. It is seen in figure 2 that the elastic part of the shear response is well described by the empirical potential up to a strain of about 0.13, close to the onset of yield. This is perhaps to be expected since the Mishin potential gives the elastic constants accurately. Figure 2 shows that while DFT results (Ogata 2002) signify the onset of yielding at a strain of 0.19, the Mishin potential allows the lattice to continue elastic deformation appreciably further, although the behaviour is clearly nonlinear. The ideal shear strength obtained using the Mishin potential is 2.91 GPa compared to 2.16 GPa for DFT. For the strain at yielding the Mishin potential value is 0.28, about 45% greater than DFT. On the basis of this comparison alone one can conclude that while the Mishin potential gives qualitatively the same stress–strain behaviour, it significantly overestimates the shearability of the metal.

To quantify the relaxation details during affine $\{111\}\langle 11\bar{2}\rangle$ shear deformation in copper we examine the interplanar spacings in the $\langle 11\bar{2}\rangle$, $\langle \bar{1}10\rangle$ and $\langle 111\rangle$ directions as a function of shear displacement. Figure 3 shows this analysis for the Mishin potential and the DFT calculations. As before, the displacement is normalized by the partial Burgers vector of the system. Both results show an expansion in the $\langle \bar{1}10\rangle$ direction, contraction in the $\langle 11\bar{2}\rangle$ direction and essentially no relaxation in the $\langle 111\rangle$ direction. The performance of the Mishin potential appears to be rather satisfactory from this comparison, in the sense that the relaxed interplanar spacing agrees with DFT results not only at small deformations ($x/b_\mathrm{p} \approx 0$) as prescribed by the elastic constants, but near the saddle point ($x/b_\mathrm{p} = 0.5$) as well. The maximum expansion

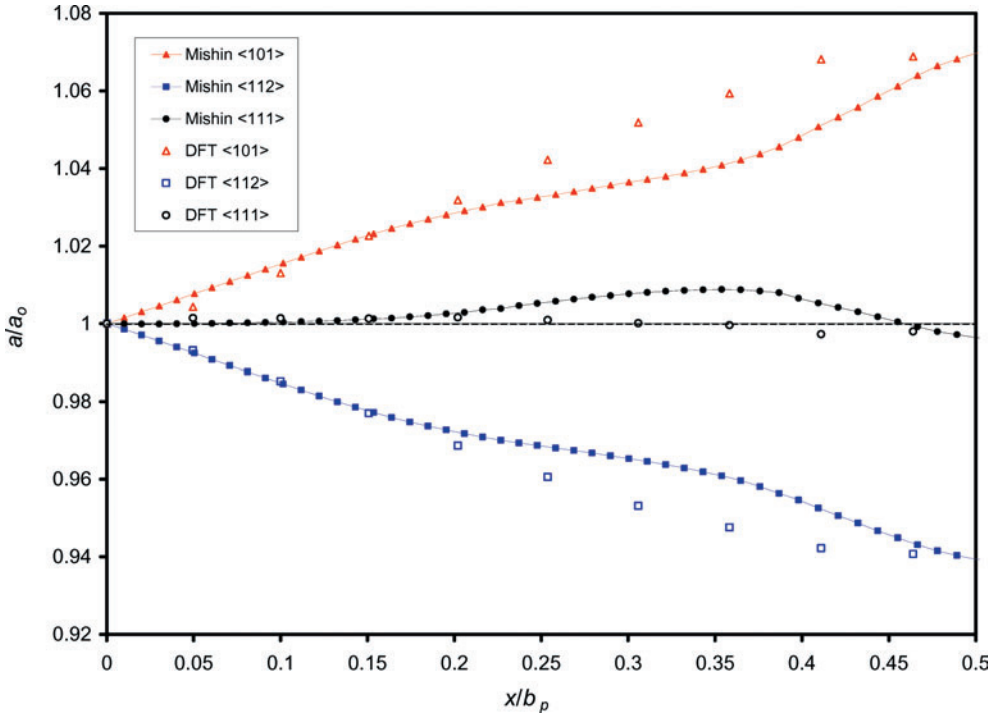

Figure 3. Atomic relaxation patterns as a function of displacement during $\{111\}\langle 11\bar{2}\rangle$ pure shear of copper are presented as interplanar distance normalized by the equilibrium interplanar spacing. Calculations were performed with the Mishin copper potential (▲, ■, ●) and DFT (△, □, ○).

in $\langle \bar{1}10\rangle$ is ∼7%, the maximum contraction in $\langle 11\bar{2}\rangle$ is ∼6%, while $\langle 111\rangle$ spacing fluctuates less than 1%.

Figure 4 shows a comparison not only between the Mishin potential and DFT results, but also between the two extreme cases of unrelaxed multiplane shear, single-plane shear ($n = 1$) and affine shear ($n = \infty$). It is seen that there is not much difference between the various cases. Since the energy is normalized by the number of planes being sheared, the similarity between $n = 1$ and $n = \infty$ indicates that the interatomic interactions are similar in the two environments. The implication is that the interaction range for atomic bonding in copper is of the order of the NN separation. In a cluster expansion of the shear deformation energy landscape, if we regard $\gamma_1(x)$ as characterizing 'double deck' or doublet interactions, then $\gamma_2(x)$ should contain additional 'triple deck' or triple interaction information, and so on. The fact that DFT gives $\gamma_1(x) \approx \gamma_\infty(x)$ for Cu suggests that doublet interactions dominate over triplet and higher order interactions in Cu. In fcc and hcp materials, an atom in the middle plane forms three NN bonds with the top plane and another three NN bonds with the bottom plane. Therefore, an equivalent statement of weak triplet interaction is that it is bond-angle (formed between two NN bonds) insensitive. Figure 5 shows the extension to the multiplane case, which would be relatively difficult to calculate with *ab initio* techniques. This result strengthens our interpretation of short-ranged and bond-angle insensitive bonding in copper, and shows that the low additional penalty due to the boundary between sheared and unsheared lattice is quickly divided among atomic planes. The $n = 15$ case is seen to be indistinguishable from the normalized penalty for affine deformation.

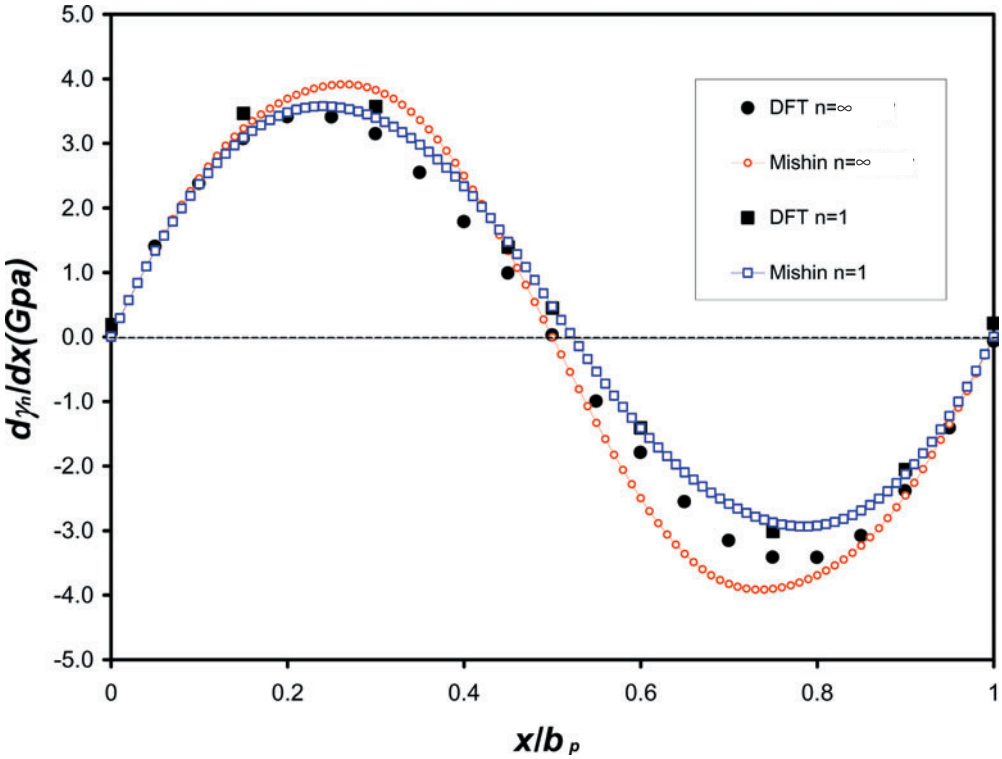

Figure 4. Unrelaxed generalized stacking fault energy for copper $\{111\}\langle 11\bar{2}\rangle$ slip calculated with the Mishin copper potential (○) and DFT (●) as well as the unrelaxed affine shear stress–displacement response computed with each method: Mishin copper potential (□) and DFT (■).

Turning to aluminium, we show in figure 6 the relaxed $\{111\}\langle 11\bar{2}\rangle$ shear stress–displacement responses calculated with the Ercolessi and Mishin potentials. The relaxed ideal shear strengths are 3.12 GPa and 1.91 GPa for the Mishin and Ercolessi potentials, respectively, compared to 2.84 GPa for DFT. Neither potential describes satisfactorily the characteristic DFT feature of an asymmetric stress–strain variation. The Mishin potential now underestimates the strain at yielding, while the Ercolessi potential displays an unphysical step behaviour at very high strains.

The relaxation patterns during $\{111\}\langle 11\bar{2}\rangle$ shear are summarized in figure 7. The Mishin potential gives relaxation results similar to DFT in an increase in the $\{111\}$ interplanar distance and a contraction in the $\langle\bar{1}10\rangle$ direction (see figure 7(*a*)). However, the potential also gives a 2% increase in the $\{11\bar{2}\}$ interplanar spacing, whereas this change was not seen in DFT. A direct correlation between the expansion in the $\langle 11\bar{2}\rangle$ direction and an artefact exhibited by the Mishin aluminium potential near the theoretical energy peak, which corresponds to $\sigma_{13} = 0$ at $x/b_p = 0.5$ (figure 6), has been observed by constraining the relaxation in that direction. This relaxation corresponds to a decrease in energy near $x/b_p = 0.5$ that creates a depression in the energy peak forming a local energy maximum at $x/b_p = 0.45$ and a local energy minimum at $x/b_p = 0.5$.

The Ercolessi potential has a more serious discontinuity that can be traced to non-physical atomic relaxation (see figure 7(*b*)). The variations in interplanar spacing in all three directions calculated with this potential show abrupt changes near $x/b_p = 0.5$ which correspond to

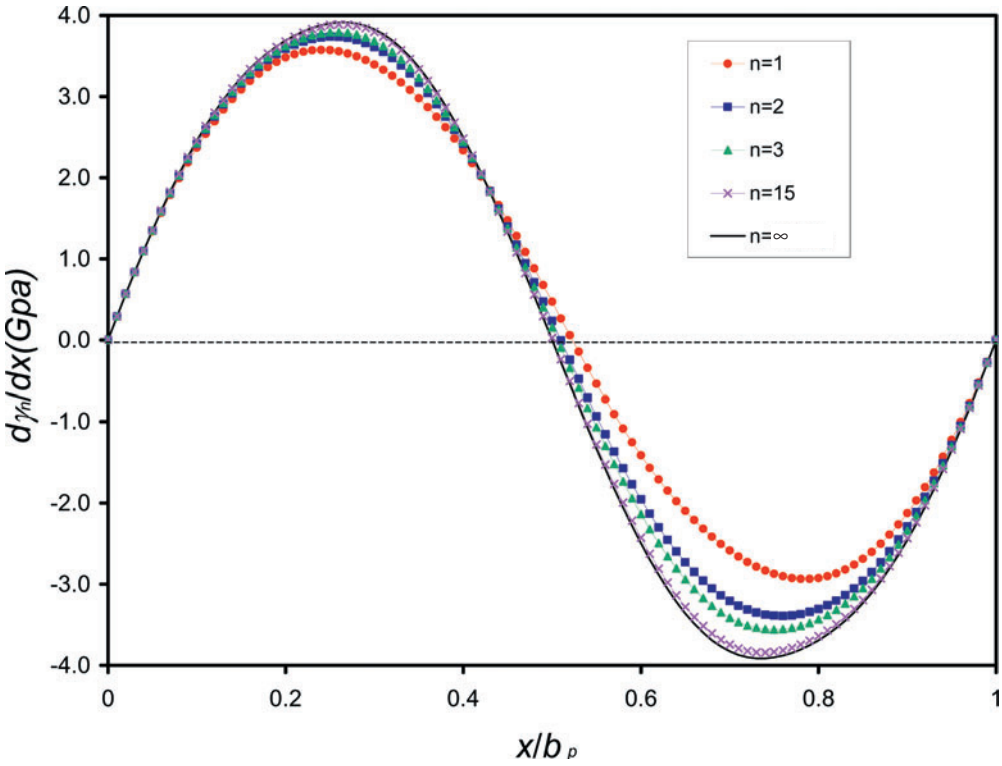

Figure 5. The multiplane generalized stacking fault energy calculated with the Mishin copper potential as stress–displacement functions, $\mathrm{d}\gamma_n(x)/\mathrm{d}x$. The $n = 15$ case is essentially overlaid on the $n = \infty$ case.

discontinuities in the second derivative of the energy with displacement. The discontinuity is associated with the energy cut-off in the Ercolessi potential at the third-NN position. The relaxation patterns do not follow the final trend until a displacement of approximately $x/b_\mathrm{p} = 0.35$ where the interplanar spacing begins to change abruptly. Up until this displacement, contraction in the $\langle 11\bar{2}\rangle$ direction and nominal expansion in the $\langle \bar{1}10\rangle$ and $\langle 111\rangle$ directions are observed. This overall relaxation behaviour is neither physically intuitive nor in agreement with DFT results and should be regarded as an artefact.

A plot of $\mathrm{d}\gamma_n(x)/\mathrm{d}x$ versus x for aluminium calculated with the Mishin potential shows significant deviation between affine shear–displacement behaviour ($n = \infty$) and the generalized stacking fault behaviour ($n = 1$) (figure 8). As the displacement, x, approaches b_p aluminium does not recover a large portion of the energy penalty incurred during shear deformation which results in an intrinsic stacking fault energy about three times that of copper. The energy recovery characteristic of aluminium is clearly reflected in the asymmetry of the shear response, $\mathrm{d}\gamma_1(x)/\mathrm{d}x$, in figure 9. Even for the $n = 15$ case, the behaviour of affine deformation has not been fully recovered. The energy maximum calculated with the Mishin potential, for the $n = 1$ case, occurs at $x/b_\mathrm{p} = 0.70$, where $\mathrm{d}\gamma_1(x)/\mathrm{d}x = 0$. This can be contrasted with the behaviour observed in copper (figure 5) where the maximum energy penalty for $n = 1$ shear occurs at $x/b_\mathrm{p} = 0.53$.

Aluminium has been shown to exhibit anisotropic electron density, which is closely associated with directional bonding (Feibelman 1990, Robertson *et al* 1993). As a result charge

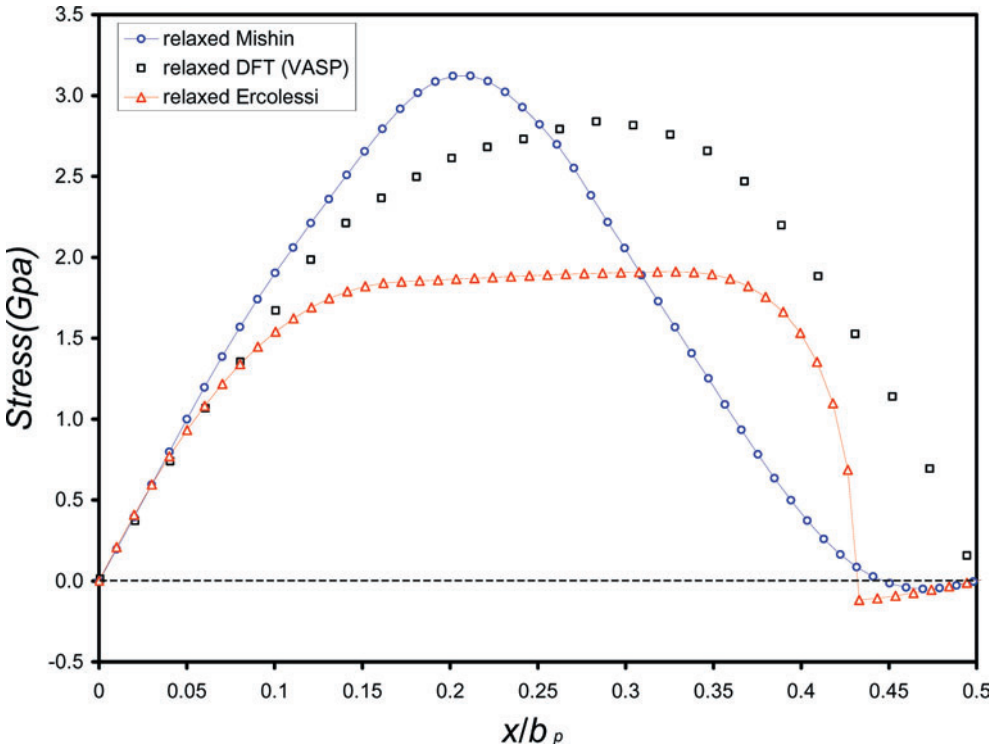

Figure 6. $\{111\}\langle 11\bar{2}\rangle$ pure shear stress–displacement response for aluminium using the Mishin aluminium potential (○), the Ercolessi aluminium potential (△) and DFT (□).

redistribution associated with breaking and reforming bonds is more difficult in aluminium than in copper (Kioussis *et al* 2002). Bonding in copper can be described as isotropic because of spherically symmetric charge density; the uniform charge density is able to adapt more quickly to the changing local environment associated with shear deformation and is therefore less sensitive to the local structure (fcc versus hcp) than it is to coordination. When an intrinsic stacking fault is formed copper is able to recover most of the energy penalty caused by shear (Ogata 2002).

4. Discussion

In this work, which deals with benchmarking the description of shear deformation using empirical interatomic potentials for copper and aluminium against first-principles calculations, we find the Mishin potential for copper accounts for the qualitative behaviour of the metal reasonably well. The potential gives good results for the detailed relaxation mechanism in affine shear and the generalized stacking fault energy. On the other hand, it does overestimate the ideal shear strength and strain. Our results reinforce the general understanding that EAM-type potentials are most applicable to metals with isotropic charge densities, as in the case of copper. The level of agreement between the Mishin potential and DFT results obtained here constitutes a best-case scenario in terms of modelling deformation behaviour beyond the database for fitting.

The Mishin potential for aluminium, which preceded the copper potential in development, has been found to be not as satisfactory. It gives a reasonable value of ideal shear strength,

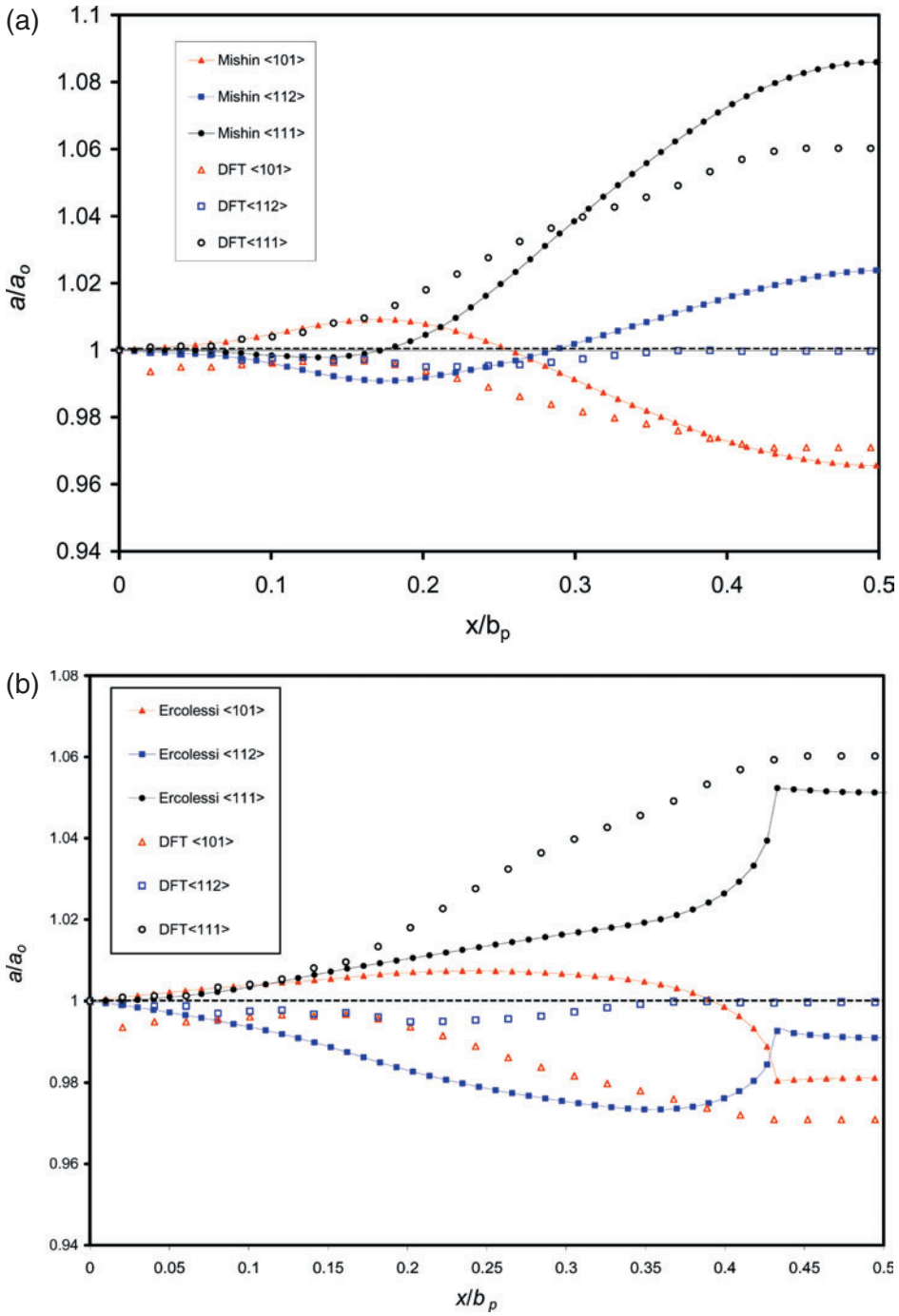

Figure 7. Atomic relaxation patterns as a function of displacement during $\{111\}\langle 11\bar{2}\rangle$ pure shear of aluminium are presented as interplanar distance normalized by the equilibrium interplanar spacing. Calculations were performed with (*a*) the Mishin aluminium potential (▲, ■, ●) and (*b*) the Ercolessi aluminium potential (▲, ■, ●) with each compared to the same DFT calculation (△, □, ○).

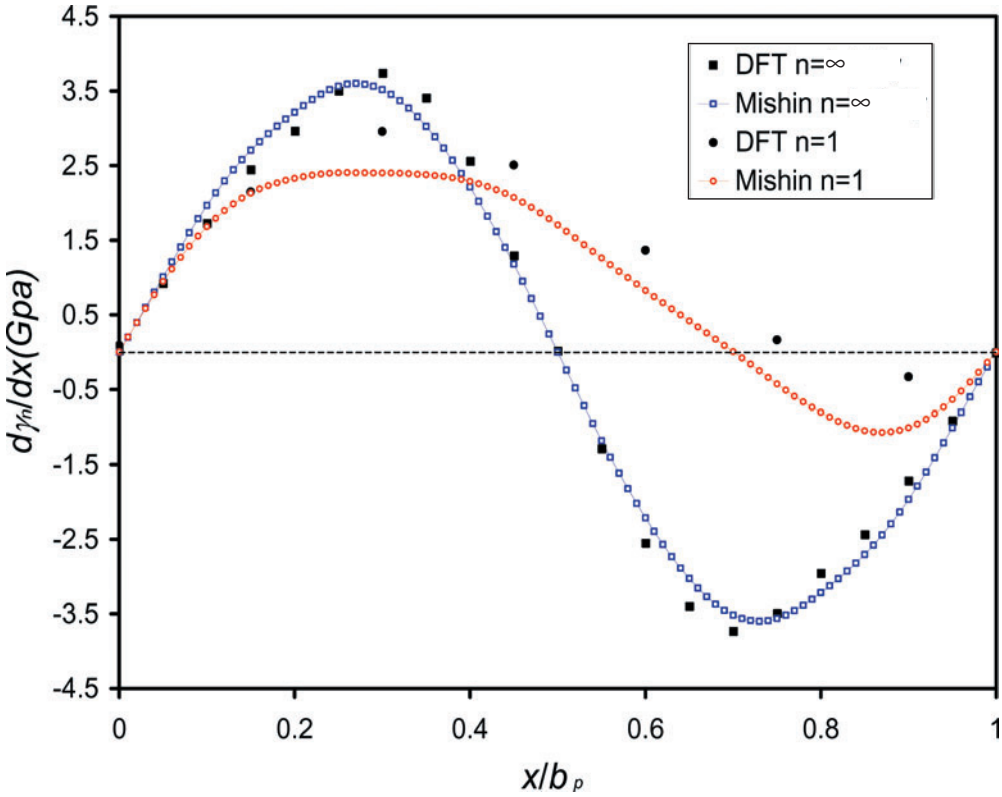

Figure 8. Unrelaxed generalized stacking fault energy for aluminium $\{111\}\langle 11\bar{2}\rangle$ slip calculated with the Mishin aluminium potential (○) and DFT (●) as well as the unrelaxed affine shear stress–displacement response computed with each method: Mishin aluminium potential (□) and DFT (■).

while appreciably underestimating the extent of nonlinear elastic deformation. The relaxation pattern was not as accurately described as in the case of copper using a different potential of essentially the same form. In describing the multiplane generalized stacking fault energy the potential qualitatively captures the asymmetry observed with DFT that we attribute to difficulty in redistributing the localized charge density in systems with directional bonding.

The Ercolessi potential for aluminium, which was developed even earlier, does not perform as well as the Mishin aluminium potential. The former significantly underestimates the ideal shear strength and gives unphysical relaxation patterns arising from an energy cut-off at the third-NN distance. The apparent agreement in relaxation patterns near the saddle point at $x/b_{\mathrm{p}} = 0.5$ with DFT results is probably fortuitous.

Our findings are consistent with a similar study benchmarking empirical EAM potentials against DFT calculations through the generalized stacking fault energy (Zimmerman *et al* 2000). While the conclusion of this study was that EAM potentials are not suited to modelling the behaviour of aluminium, we feel that our results show that the Mishin potential does capture some of the significant behaviour observed in DFT calculations. Several copper potentials were evaluated in the previous study; however, the Mishin potential for copper had not appeared at the time. On the basis of the present benchmark of shear deformation, we regard the Mishin copper potential as the most accurate interatomic potential available at present for this metal.

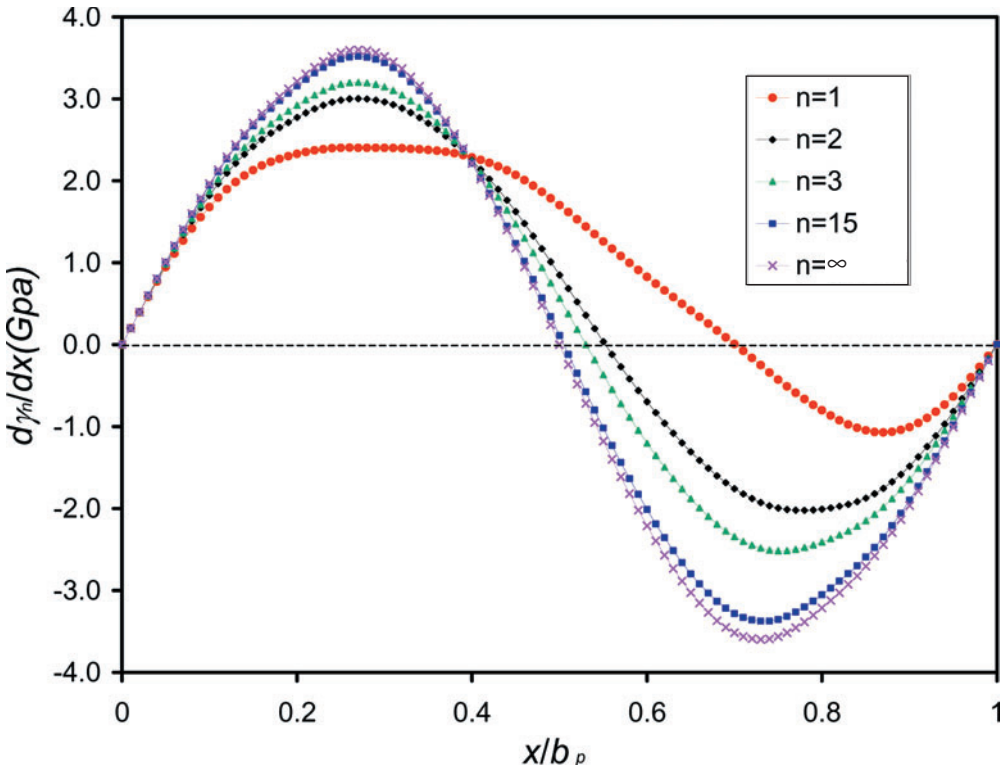

Figure 9. The multiplane generalized stacking fault energy calculated with the Mishin aluminium potential as stress–displacement functions, $\mathrm{d}\gamma_n(x)/\mathrm{d}x$. Aluminium shows significant asymmetry for the $n = 1$ case and has not converged to the affine case even at $n = 15$.

When comparing copper with aluminium, DFT shows aluminium to have higher ideal shear strength and a longer range of elastic deformation before the onset of plasticity (Ogata 2002). The Mishin potentials for these two metals give the same order of the ideal shear strengths while showing copper to have the longer range of elastic deformation. We attribute this to the difficulty of treating directional bonding or angle-dependent forces with EAM-type formulations. We observe that an EAM potential of the form of equation (1), though it involves no explicit angular variables, can still represent angular dependence implicitly, if the potential cut-off is chosen to include many neighbouring shells, and if the fitting is done carefully. The reason is because angular information is inferable from distance information. For example, if the lengths of all three sides of a triangle are known, the three angles are also known (triangulation). Thus, with flexible choices for $G_i(\rho)$ and $V(r_{ij})$, one may consciously or unconsciously 'fold in' angular dependence into these radial functions. However, an unfortunate consequence of this in a setting of large-scale numerical optimization of the potential parameters is that one may no longer understand the outcome of fitting. Both the Mishin and the Ercolessi potentials for aluminium contain oscillations of unclear physical origin in the pair- and/or embedding functions, which are absent in almost all the empirical potentials for Cu. Thus one may suspect that strong angle-dependent effects in Al have been vaguely 'folded in' into the $G_i(\rho)$ and $V(r_{ij})$ functions through the numerical fitting procedure.

The above view, however, could be too narrow. Dagens *et al* have shown that in a perturbational limit where interatomic interaction reduces to a sum of pair interactions, Al does

have a longer-ranged pair potential with oscillations (Dagens *et al* 1975). Thus, should we describe the abnormal behaviour of Al as due to 'long-ranged angle-independent' interactions, or 'short-ranged but angle-dependent' interactions like those in Baskes (1992), Lee *et al* (2001) and Li *et al* (2003)? The answer is probably that only the N-body Born–Oppenheimer (BO) surface is a true physical measurable. Interatomic potentials are merely cluster expansion schemes to approximate the true BO surface, and individual terms in a potential model are not physical measurables. Thus, choosing to use 'long-ranged angle-independent' terms or 'short-ranged but angle-dependent' terms in expanding the BO surface becomes a matter of most easily capturing the essential behaviour of interest while maintaining computational efficiency, not always an easy task. Baskes *et al* have shown that both EAM (long-ranged angle-independent) and modified-EAM (short-ranged but angle-dependent) potentials give reasonable descriptions of defects in Al (Baskes 2001). However, in the limit of a large enough basis, all types of cluster expansion schemes should give not just reasonable descriptions, but the same converged result for the BO surface, at least theoretically.

Lastly, we would like to point out the usefulness of rigorously benchmarking empirical potentials against *ab initio* calculations. Many problems of interest are inaccessible owing to the length and time scales of *ab initio* calculations. However, by thoughtfully comparing the results of simple calculations obtainable with both empirical potentials and *ab initio* calculations, simulations using empirical potential can be more thoroughly understood. It is important in this process to choose benchmark calculations that accurately reflect the behaviour of interest to the larger-scale simulations. The current work explores the detailed behaviour under shear deformation of fcc metals, with the goal of better understanding molecular dynamics simulations of deformation and defect nucleation in these metals (Van Vliet *et al* 2003, Choi *et al* 2003, Zhu *et al* 2004, Kimizuka *et al* 2004). An accurate understanding of the successes and limitations of empirical potentials allows for a more informed interpretation of the results of simulations using these potentials.

Acknowledgments

SO thanks Prof. Y Shibutani and Prof. H Kitagawa. JL acknowledges support from Honda R&D Co., Ltd and the OSU Transportation Research Endowment Program. RDB and SY both acknowledge support from the Lawrence Livermore National Laboratory; in addition SY acknowledges support from Honda R&D, DARPA/ONR, NSF and AFOSR.

References

Baskes M I 1992 Modified embedded-atom potentials for cubic materials and impurities *Phys. Rev.* B **46** 2727

Baskes M I 2001 Determining the range of forces in empirical many-body potentials using first-principles calculations *Phil. Mag.* A **81** 991

Choi Y, Van Vliet K J, Li J and Suresh S 2003 Size effects on the onset of plastic deformation during nanoindentation of thin films and patterned lines *J. Appl. Phys.* **94** 6050

Dagens L, Rasolt M and Taylor R 1975 Charge densities and interionic potentials in simple metals: nonlinear effects *Phys. Rev.* B **11** 2726

Ercolessi F and Adams J B 1994 Interatomic potentials from first-principles calculations: the force-matching method *Europhys. Lett.* **26** 583

Feibelman P J 1990 Diffusion path for Al adatom on Al(001) *Phys. Rev. Lett.* **65** 729

Hohenberg P and Kohn W 1964 Inhomogeneous electron gas *Phys. Rev.* **136** B864

Kioussis N, Herbranson M and Collins E 2002 Topology of electronic charge density and energetics of planar faults in fcc metals *Phys. Rev. Lett.* **88** 125501

Kimizuka H, Kaburaki H, Shimizu F, Li J and Yip S 2004 Crack-tip nanostructures of dislocations in the fracture process of fcc metals: a molecular-dynamics study *J. Computer-Aided Mater. Design* at press

Kohn W and Sham L J 1965 Self-consistent equations including exchange and correlation effects *Phys. Rev.* **140** A1133

Kresse G and Hafner J 1993 *Ab initio* molecular dynamics for liquids *Phys. Rev.* B **47** 558

Lee B J, Baskes M I, Kim H and Cho Y K 2001 Second nearest-neighbor modified embedded atom method potentials for bcc transition metals *Phys. Rev.* B **64** 184102

Li J, Liao D, Yip S, Najafabadi R and Ecker L 2003 Force-based many-body interatomic potential for ZrC *J. Appl. Phys.* **93** 9072

Methfessel M and Paxton A T 1989 High-precision sampling for brillouin-zone integration in metals *Phys. Rev.* B **40** 3616

Mishin Y, Faraks D, Mehl M J and Papaconstantopoulos D A 1999 Interatomic potentials for monoatomic metals from experimental data and *ab initio* calculations *Phys. Rev.* B **59** 3393

Mishin Y, Mehl M J, Papaconstantopoulos D A, Voter A F and Kress J D 2001 Structural stability in lattice defects in copper: *ab initio*, tight-binding and embedded-atom calculations *Phys. Rev.* B **63** 224106

Monkhorst H J and Pack J D 1976 Special points for brillouin-zone integrations *Phys. Rev.* B **13** 5188

Ogata S, Li J and Yip S 2002 Ideal pure shear strength of aluminum and copper *Science* **298** 807

Perdew J P *et al* 1992 Atoms, molecules, solids, and surfaces: applications of the generalized gradient approximation for exchange correlations *Phys. Rev.* B **46** 6671

Press W H, Teukolsky S A, Vetterling W T and Flannery B P (ed) 1996 *Numerical Recipes in Fortran 90: The Art of Scientific Computing* (Cambridge: Cambridge University Press)

Robertson I J, Heine V and Payne M C 1993 Cohesion in aluminum systems: a first-principles assessment of 'glue' schemes *Phys. Rev. Lett.* **70** 1944

Vanderbilt D 1990 Soft self-consistent pseudopotentials in a generalized eigenvalue formalism *Phys. Rev.* B **41** 7892

Van Vliet K J, Li J, Zhu T, Yip S and Suresh S 2003 Quantifying the early stages of plasticity through nanoscale experiments and simulations *Phys. Rev.* B **67** 104105

Vitek V 1968 Intrinsic stacking faults in body-centered cubic crystals *Phil. Mag.* **18** 773

Voter A F 1994 *Intermetallic Compounds: Principles* vol 1 (New York: Wiley) p 77

Zhu T, Li J, Van Vliet K J, Ogata S, Yip S and Suresh S 2004 Predictive modeling of nanoindentation-induced homogeneous dislocation nucleation in copper *J. Mech. Phys. Solids* **52** 691

Zimmerman J A, Gao H and Abraham F F 2000 Generalized stacking fault energies for embedded atom fcc metals *Modelling Simul. Mater. Sci. Eng.* **8** 103